



# Influence of the Madden-Julian Oscillation on the diurnal cycles of convection and precipitation over the Congo Basin

Kathrin Alber<sup>\*</sup>, Liming Zhou, Paul E. Roundy, Stephen L. Solimine

Department of Atmospheric and Environmental Sciences, University at Albany, State University of New York, Albany, NY 12222, USA

## ARTICLE INFO

### Keywords:

Congo rainforest  
Diurnal cycle  
Madden-Julian Oscillation  
Precipitation  
Tropical convection

## ABSTRACT

The Congolese rainforest is a hotspot for convection where thunderstorms and rainfall exhibit a strong diurnal cycle. Previous studies have shown that various modes of variability such as the Madden-Julian Oscillation (MJO), the leading mode of intraseasonal variability in the tropics, can impact the diurnal cycles of precipitation and convection over tropical land areas. Thus, this study analyzes the influence of the MJO on diurnal variations of convection and precipitation over the Congo and explores possible mechanisms leading to the observed changes, using Gridded Satellite (GridSat-B1), Tropical Rainfall Measuring Mission (TRMM), and ERA5 reanalysis data. Results show that convection and precipitation are increased during the MJO enhanced convective phase (RMM phases 1 and 2) and decreased during the suppressed convective phase (RMM phases 5 and 6), where the differences are found to be largest during the morning hours when convection is weakest. Convection is generally deeper during the enhanced phase and shallower during the suppressed phase, accompanied by a slower decay of convective clouds and anvils during the enhanced phase. Furthermore, the influence of the MJO was found to be stronger on stratiform precipitation compared to convective precipitation. While the diurnal cycles of convective precipitation fractions are similar during both MJO phases, the fraction of stratiform precipitation is higher during the enhanced phase, mainly in the morning hours. Suggested atmospheric drivers contributing to the observed differences between the two MJO phases include enhanced upward air motion in the mid- and upper levels and strong divergence in the upper levels during the enhanced phase, and strong mid-level divergence and upper- to mid-level subsidence during the suppressed phase, mainly during the nighttime and morning hours. Furthermore, decreased mid-level wind speed, increased upper-level wind speed, and enhanced relative humidity may be contributing factors to the increased formation of stratiform precipitation during the enhanced phase. These results enhance our understanding of the MJO's impacts on precipitation and convection variability, ultimately improving predictions of MJO modulated rainfall over the Congo.

## 1. Introduction

The Congo Basin situated in equatorial tropical Africa is one of the most convective regions in the world and has the second largest latent heating rate from convection after the Maritime continent (MC) (Washington et al., 2013; Feng et al., 2021). Convection and rainfall over the Congo are predominately associated with surface solar heating, resulting in a strong diurnal cycle of clouds and precipitation with a minimum in clouds in the morning and a peak in clouds and convection in the late afternoon and early evening hours (Jackson et al., 2009; Alber et al., 2021a; Hartman, 2021). Several previous studies have shown that convection varies diurnally, and that the diurnal variations also differ spatially. Different techniques and datasets have been utilized to

investigate the diurnal cycles of tropical convection and precipitation. For example, Hendon and Woodberry (1993) used brightness temperature ( $T_b$ ) derived from 11  $\mu\text{m}$  satellite radiance measurements lower than 230 K as a threshold to isolate deep convection. Nesbitt and Zipser (2003) used Tropical Rainfall Measuring Mission (TRMM) satellite precipitation measurements to highlight variations in rainfall over tropical land areas, while Yang and Slingo (2001) used global 0.5° and 3-hourly satellite infrared data to provide a climatology of the diurnal cycle of convection and surface temperature in the tropics.

According to Lazri et al. (2014), the life cycle of a convective system can generally be divided into three stages, i.e., growth, maturity, and dissipation. The cycle begins with the vertical growth of a convective core with intensifying vertical updrafts. During this stage, the cloud top

<sup>\*</sup> Corresponding author.

E-mail address: [kalber2@albany.edu](mailto:kalber2@albany.edu) (K. Alber).

<https://doi.org/10.1016/j.atmosres.2023.106967>

Received 24 December 2022; Received in revised form 8 August 2023; Accepted 13 August 2023

Available online 14 August 2023

0169-8095/© 2023 Elsevier B.V. All rights reserved.

height increases, the cloud expands horizontally, and the cloud optical thickness increases while precipitation droplets grow. During the maturity stage, both updrafts and downdrafts exist simultaneously, where evaporating precipitation cools surrounding areas which favors downdrafts while the anvil expands. During the dissipation stage, updrafts weaken and begin to disappear while the anvil reaches a maximum and begins to dissipate and the cloud droplet radius decreases. In the young portions of the cloud, defined by vigorous vertical motion, precipitation is mostly convective where precipitation particles increase the size and mass by collection of cloud water through coalescence and/or riming and the particles fall in heavy showers. In the older regions of the cloud when the vertical motions weaken, precipitation is more stratiform and drifts to the ground more slowly as the particles increase their mass by vapor diffusion (Houze Jr., 1997).

Precipitation and convection over the tropics can be influenced by various modes of variability such as the Madden-Julian Oscillation (MJO), El Niño Southern Oscillation (ENSO) and Indian Ocean Dipole (IOD) (Otto et al., 2013; Hart et al., 2019; Raghavendra et al., 2020; Jiang et al., 2021). The MJO (Madden and Julian, 1971, 1972) is one of the most fundamental modes of atmospheric variability and is the leading mode of intraseasonal variability in the tropics (Dias et al., 2017). It is characterized as an eastward moving planetary-scale signal, associated with strong convection that originates in the Indian Ocean and moves along the equatorial Indian and western-central Pacific Oceans, recurring every 30–90 days (Zhang, 2005; Kim et al., 2008). Convection is increased during the MJO enhanced phase and decreased during the MJO suppressed phase. It has also been shown that the MJO interacts with the diurnal cycle (Slingo et al., 2003; Sakaeda et al., 2017). However, the modulation of precipitation by the MJO varies in different regions of the world, and studies disagree on how the MJO affects the diurnal cycle phase and amplitude of rainfall and convection depending on the region. While the diurnal amplitude is found to be decreased during the MJO enhanced phase over the islands of the MC, it is shown to increase over the oceans of the MC during the same phase (Sui and Lau, 1992; Sui et al., 1997; Rauniyar and Walsh, 2011; Oh et al., 2012), suggesting that the MJO impacts the diurnal cycles of rainfall and convection differently over land and the ocean. Furthermore, studies analyzing the influence of the MJO on the diurnal phase show contradictory results. For example, Oh et al. (2012) and Rauniyar and Walsh (2011) identified the MJO's influence on the diurnal phase, while Tian et al. (2006) and Suzuki (2009) found no relationship between the two at all.

Over the Congo, Raghavendra et al. (2020) found a significant relationship between the MJO and rainfall during October through March from 1979 to 2018, showing that the MJO significantly impacts rainfall over the region. They utilized the daily MJO real-time multi-variable (RMM) phase index data (Wheeler and Hendon, 2004), where RMM phase 2 was regarded as the MJO enhanced phase and RMM phases 5 and 6 were regarded as the MJO suppressed phase over the region. The study showed that the number of days in the MJO suppressed phase increased significantly by 0.34 days year<sup>-1</sup> from 1979 to 2018, while no significant trends for the number of MJO enhanced days were found. The study concluded that the decreasing trend in the number of MJO dry days may contribute to the observed decrease in rainfall by 13.6% and may thereby help to partially explain the large-scale and long-term drying trend documented during the past three decades over the Congo (Zhou et al., 2014; Hua et al., 2016, 2018; Jiang et al., 2019). Interestingly, in contrast to this drying trend, several studies such as Taylor et al. (2018), Raghavendra et al. (2018), and Alber et al. (2021b) also showed an increase in thunderstorm intensity over the Congo during the past 20 to 30 years.

However, despite being the second largest rainforest on earth, the Congo remains understudied compared to other major rainforests such as the Amazon (Zhou et al., 2014; Alsdorf et al., 2016). Although the impacts of the MJO on African climate has been analyzed, most studies have focused on Eastern Africa (e.g., Pohl and Camberlin, 2006; Berhane

and Zaitchik, 2014; Vashisht and Zaitchik, 2022; Maybee et al., 2022; Talib et al., 2023), Southern Africa (e.g., Hart et al., 2013) or Western Africa (e.g., Alaka and Maloney, 2012; Sossa et al., 2017). To the best of our knowledge, no studies have been conducted yet to investigate how the MJO may influence the diurnal variations of convection and rainfall over the Congo. This study therefore aims to shed light on the yet unanswered question of how the MJO might impact the diurnal cycles of convection and precipitation over the Congo and investigates the physical mechanisms leading to the observed changes. The results of this analysis will fill the knowledge gap regarding the variability of Congo rainfall and convection and may ultimately help to answer open questions about the long-term drying trend over the Congo. The data used is presented in Section 2, the methods are described in Section 3, the results are presented in Section 4, followed by a summary and conclusion in Section 5.

## 2. Data

For this study, three different datasets were used, i.e., Gridded Satellite (GridSat-B1) (Knapp, 2008; Knapp et al., 2011), TRMM precipitation (Huffman et al., 2007), and ERA5 reanalysis data (Hersbach et al., 2020), where the time period 1985–2019 was investigated. Although the MJO impacts convection and precipitation during all seasons, the months October through March (ONDJFM) were chosen for the analysis because the MJO signal is stronger and the RMM amplitude is generally higher during these months (Zhang and Dong, 2004; Raghavendra et al., 2020). Additionally, this period includes both the wet and dry seasons over the Congo since the analysis captures the entire December–February (DJF) dry season, the start of the March–May (MAM) wet season, and most of the September–November (SON) wet season (Nicholson, 2018), resulting in the analysis capturing three wet months and three dry months. It is worth noting that the MJO's impacts on convection do not differ significantly between the three dry vs. wet months and we therefore decided to combine these 6 months into one single ONDJFM study period for brevity and clarity. Comparing the modulation of convection by the MJO during all four seasons, i.e., DJF, MAM, JJA, and SON (not shown), also indicated similar results for all seasons besides JJA when the differences between the two MJO phases are more pronounced from noon through the afternoon instead of the nighttime and morning hours. The study domain, i.e., the Congo Basin, is defined as the area from 5°N to 5°S and 12°E to 30°E and is depicted by the black boxes in Fig. 1. The diurnal cycle data are indicated in Coordinated Universal Time (UTC).

### 2.1. GridSat-B1 satellite data

The GridSat-B1 infrared channel (11 μm) brightness temperature ( $T_b$ ) dataset derived from the International Satellite Cloud Climatology Project (ISCCP; Schiffer and Rossow, 1983) was used in this study to identify convective clouds. This Climate Data Record quality, long-term  $T_b$  dataset was sampled from the European Meteorological (MET) series of geostationary satellites. Since the atmosphere is almost transparent at 11 μm, the satellite measured radiance was utilized to derive  $T_b$  for cloud top (i.e., cloudy-sky) or surface (i.e., clear-sky) temperatures. The dataset is available at a 0.07° × 0.07° spatial and 3-hourly temporal resolution from 1981 to present (Knapp, 2008; Knapp et al., 2011). However, only the data from 1985 to 2019 was used here due to the high frequency of missing data between 1982 and 1985 (Raghavendra et al., 2020).

### 2.2. TRMM precipitation data

TRMM satellite precipitation estimates, i.e., TRMM 3B42 and TRMM 2A23, were analyzed to investigate the diurnal cycle of precipitation. The TRMM satellite was launched in November 1997, carrying a precipitation radar (i.e., an active microwave sensor), allowing the

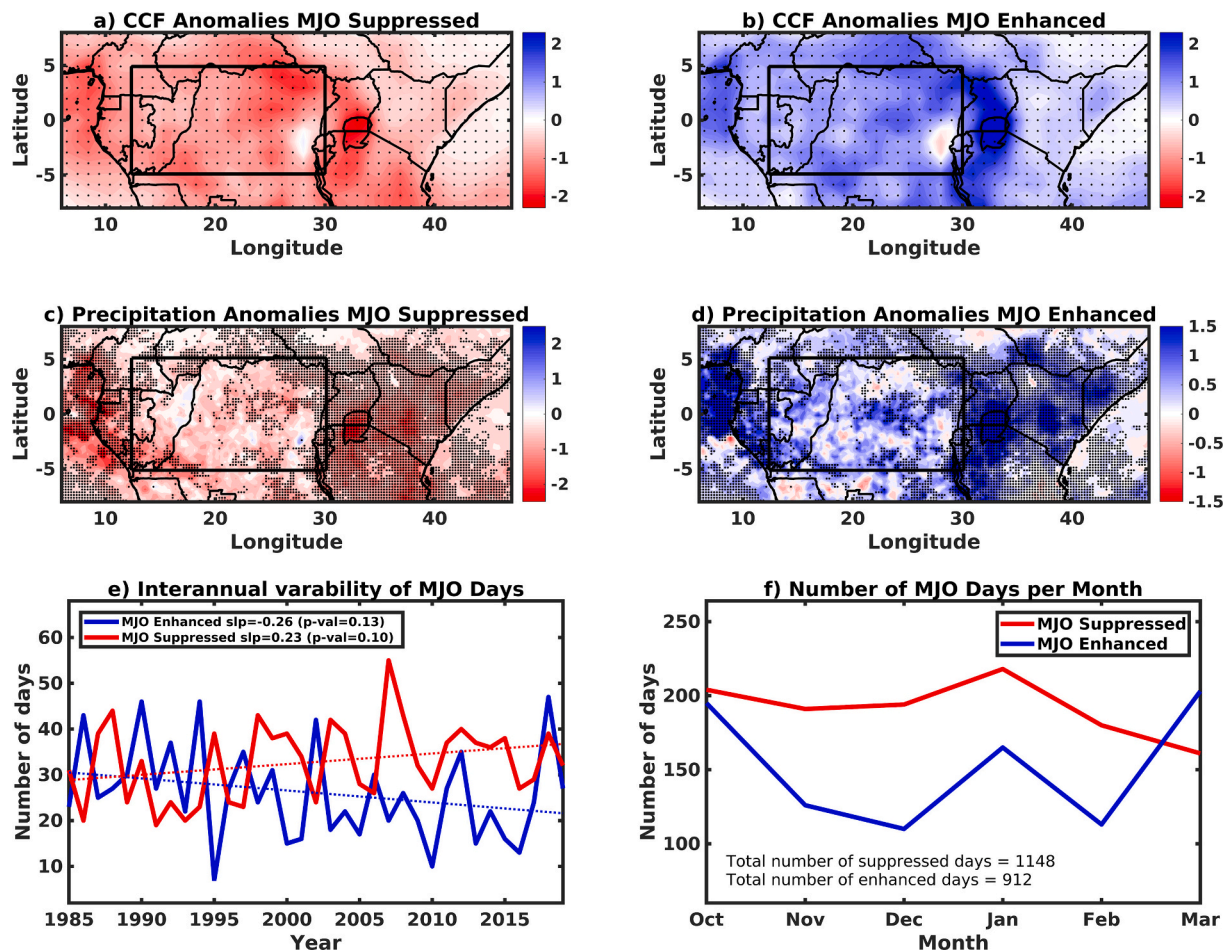


**Fig. 1.** (a–d): Anomalies of (a), (b) 3-hourly GridSat-B1 CCF (%) and (c), (d) daily TRMM precipitation (mm) for the MJO enhanced phase (top) and the MJO suppressed phase (middle) from 1985 to 2019. The study region (i.e., the Congo Basin) is represented by the black box. The black dots indicate that the values during the enhanced and suppressed phase are significantly different from each other at  $p < 0.05$  (determined using a two-sample ttest). (e): Interannual variability of the number of enhanced (blue) and suppressed (red) MJO days over the study region during ONDJFM. (f): Number of enhanced (blue) and suppressed (red) MJO days per month from 1985 to 2019, averaged over the study region. (For interpretation of the references to colour in this figure legend, the reader is referred to the web version of this article.)

sampling throughout the diurnal cycle (Zipser et al., 2006). For the TRMM 3B42, rainfall estimates were acquired from NASA’s Goddard Earth Sciences Data and Information Services Center ([https://disc.gsfc.nasa.gov/datasets/TRMM\\_3B42\\_7/summary](https://disc.gsfc.nasa.gov/datasets/TRMM_3B42_7/summary)), available from 1998 to 2019 at a 3-hourly temporal resolution and a  $0.25^\circ \times 0.25^\circ$  spatial resolution. Studies such as Munzimi et al. (2015) and Nicholson et al. (2019) showed that the dataset performs well over the Congo. Additionally, the TRMM precipitation radar rain characteristics (TRMM 2A23) version 7 orbital data were used to provide rain type classification information, i.e., stratiform and convective precipitation. The dataset was acquired from the University of Washington TRMM Database (UWTD) (<http://trmm.atmos.washington.edu>), available from 1998 to 2013 and interpolated to a  $0.05^\circ \times 0.05^\circ$  spatial resolution and to a 1-hourly temporal resolution.

The differentiation between stratiform and convective precipitation in the TRMM 2A23 dataset was made using an algorithm developed by Awaka et al. (1997), where the precipitation type was classified into “stratiform”, “convective” and “other” by using two different methods, i.e., the vertical profile method (V-method) and the horizontal pattern method (H-method). The V-method first attempts to detect a bright band (BB) and the precipitation is classified as stratiform if a BB is found. If no BB is detected, the algorithm looks for a strong radar echo which will classify the precipitation as convective. If neither a BB nor a strong radar echo is detected, the precipitation is classified as “other”. For the H-

method, the radar first aims to detect a convective core and then classifies the precipitation type around the core by examining horizontal patterns of the maximum reflectivity factor. The precipitation classification performed by the two methods is then merged and a final classification is made (Awaka et al., 1997).

It is worth pointing out that the TRMM precipitation data is estimated during the passage of the TRMM satellite over the study region. Thus, the values are relative due to the low sampling frequency of TRMM which is about 0.5 times  $\text{day}^{-1}$  near the equator, making it imperative to use measurements over several years to be able to sample the diurnal cycle (Jackson et al., 2009).

### 2.3. ERA5 reanalysis

The ERA5 reanalysis dataset (Hersbach et al., 2020) was used to obtain the variables needed to calculate the Gálvez-Davison Index (GDI), i.e., temperature and specific humidity data at 950 hPa, 850 hPa, 700 hPa, and 500 hPa (see Section 3.3 for a more detailed explanation of the GDI). Additionally, divergence, vertical velocity, U and V wind, relative humidity, and temperature data were acquired in intervals of 50 hPa from 100 hPa to 1000 hPa. For comparison to the TRMM satellite precipitation, ERA5 total precipitation was obtained as well. The data was used at a  $0.25^\circ \times 0.25^\circ$  spatial resolution and an hourly temporal resolution from 1985 to 2019 to match the timespan utilized for the



GridSat-B1 data. Due to the scarcity of surface observations (e.g., gauge stations and radiosonde networks) over the Congo, it is difficult to identify the most accurate reanalysis dataset over the region. However, it has been shown that the bias and root-mean-square error associated with the ERA-Interim reanalysis dataset is comparable with other reanalysis products over the region (Hua et al., 2019). Additionally, Gleixner et al. (2020) found that the correlation in temperature and precipitation between the ERA5 data and observations improved when compared to the ERA-Interim reanalysis data over Africa.

### 3. Methods

#### 3.1. MJO Identification

The daily MJO real-time multivariable (RMM) phase index data (Wheeler and Hendon, 2004) from the Bureau of Meteorology in Australia (<http://www.bom.gov.au/climate/mjo/>) was used to identify the phases of the MJO. The RMM index, based on a pair of empirical orthogonal functions (EOFs) of the combined fields of outgoing long-wave radiation (OLR), 850 hPa and 200 hPa zonal winds averaged from 15°N to 15°S, is widely used to monitor the MJO (Wheeler and Hendon, 2004). Days with an RMM index amplitude  $>1$  were regarded as active MJO days, while days with an RMM index amplitude  $<1$  were considered as inactive MJO days (LaFleur et al. 2015). RMM phases 1 and 2 were defined as the MJO enhanced convective phase, and phases 5 and 6 were considered as the MJO suppressed convective phase over the Congo (Gottschalck et al., 2010; Zaitchik, 2017). A total of 912 days were identified as MJO enhanced days while 1148 days were identified as MJO suppressed days.

#### 3.2. GridSat-B1 cloud fraction

To quantify convection, the cold cloud fraction (CCF) was derived from the GridSat-B1 data, by calculating the fraction of grid points with  $T_b < -50$  °C within the study domain (e.g., Raghavendra et al., 2018; Alber et al., 2021b). The CCF represents areas in which deep convection occurs since tropical deep convection is characterized by very cold  $T_b$  values (Taylor et al., 2017; Hart et al., 2019). Additionally, the cloud fractions with  $T_b > -50$  °C and  $< -25$  °C, and  $T_b > -25$  °C and  $< 0$  °C were calculated to investigate the diurnal cycles of warmer clouds.

#### 3.3. Gálvez-Davison Index

For comparison to the GridSat-B1 CCF, the GDI was derived from the ERA5 reanalysis data to estimate convection. The GDI is calculated by using temperature and specific humidity values at 4 different levels (i.e., 950 hPa, 850 hPa, 700 hPa, and 500 hPa), where ERA5 temperature and specific humidity data was used for the calculation in this study. The GDI is a thermodynamic index, developed by Michael Davison and José Gálvez at NOAA's Weather Prediction Center (WPC) (Gálvez and Davison, 2016), aiming to improve forecasts of tropical convection since the skill of traditional stability indices is limited in the tropics. The GDI focusses on thermodynamic processes in the mid- and low troposphere rather than dynamical processes and consists of several different sub-indices evaluating different processes that dominate the variability of convection. It consists of three different sub-indices, the Column Buoyancy Index (CBI) considering the availability of heat and moisture in the middle and lower troposphere, the Mid-Tropospheric Warming Index (MWI) accounting for the stabilizing and destabilizing effects of mid-level ridges and troughs, and the Inversion Index (II) analyzing the entrainment of dry air and stabilization associated with trade wind inversions. The higher the GDI value, the more intense and more likely are thunderstorms and convection. Alber et al. (2021b) showed that trends in the GDI over the Congo are consistent with trends in CCF, and Miller et al. (2019) found that the GDI's skill is considerably higher in forecasting rainfall over Puerto Rico than other stability indices such as

CAPE or the K-Index. A complete derivation of the GDI can be found in Gálvez and Davison (2016) and Alber et al. (2021b).

#### 3.4. Diurnal cycle calculation

To quantify the impacts of the MJO on the diurnal cycles of convection and precipitation, the diurnal cycles of the GridSat-B1 CCF, the ERA5 derived GDI, and TRMM and ERA5 precipitation for the MJO enhanced and suppressed phases were calculated. To highlight the impacts of the MJO on the diurnal cycles, the relative mean differences (RMD) between MJO enhanced and suppressed phases were further calculated by dividing the difference between the two phases by the climatological mean, resulting in a dimensionless quantity. To calculate the diurnal cycles for different variables, the discrete Fourier transform (DFT) was applied to the anomaly data using a fast Fourier transform (FFT) and a 3–24-h spectral filter was applied. Additionally, the 95% confidence intervals of the diurnal cycles were derived by multiplying the standard error with the 95% probability intervals at each timestep. The diurnal cycles of convective and stratiform precipitation derived from the TRMM 2A23 data were calculated by dividing the stratiform and convective precipitation fraction, respectively, by the daily sum of all precipitation, resulting in the stratiform and convective precipitation data being displayed as percentage of the daily total precipitation. As suggested by Negri et al. (2002), a 4-h smoothing was then applied to reduce errors due to the high sampling variability of the TRMM data. Because of the high frequency of missing values in the TRMM 2A23 dataset, the diurnal cycles of stratiform and convective precipitation were calculated using climatological means and were not derived using Fourier analysis. To investigate the physical mechanisms leading to the observed changes in precipitation and deep convection, the time-height cross sections of divergence, vertical velocity, relative humidity, wind speed, and temperature were calculated for the MJO suppressed and enhanced phases, where the according values were averaged over all MJO enhanced days and all MJO suppressed days, respectively. Additionally, the difference between the two MJO phases for each variable was computed separately. To highlight the variations across the day, the diurnal variations of the differences were calculated as follows: For each pressure level, the diurnal average of the difference was calculated first. Then, the diurnal average was subtracted from the difference at each hour and according pressure level.

### 4. Results

#### 4.1. Spatial and temporal anomalies associated with the MJO phases

The MJO enhanced and suppressed phases are associated with different cloud and rainfall anomaly patterns over the Congo rainforest (Fig. 1a–d). During the MJO suppressed phase, a decrease in CCF and a decrease in precipitation of up to  $2 \text{ mm day}^{-1}$  across some parts of the Congo Basin can be observed over the study region, with the exception of a very small area of slightly increased CCF and precipitation values along the western rift valley and some small areas of increased precipitation areas scattered through the study region (Fig. 1a and c). During the enhanced phase, CCF and precipitation are increased over most of the study area, where precipitation increases by up to  $1.5 \text{ mm day}^{-1}$  in some parts of the study area. Some exceptions include the same area along the western rift valley, showing slightly decreased CCF values (Fig. 1b), and smaller patches of decreased precipitation throughout the study domain including along the rift valley (Fig. 1d). The anomalies along the western rift valley could be a result of the unique topography in that region, where the altitude increases  $>1000$  m from the Congo Basin up to the East African Highlands. It is also worth noting the strong MJO induced precipitation anomalies outside the study domain along the golf of Guinea, which could be an area of future research, where Zaitchik (2017) suggests that the influence of the MJO on West African rainfall might be linked to African Easterly Wave activity during boreal

summer.

As for the temporal variations of the number of enhanced and suppressed MJO days, Fig. 1e shows that the number of suppressed MJO days has been increasing from 1985 to 2019, while the number of enhanced MJO days has been decreasing slightly but insignificantly. As suggested by Raghavendra et al. (2020), the increase in MJO suppressed days could be a contributing factor to the decrease in precipitation and therefore the drying trend observed over the region. In Fig. 1f, the temporal variability of MJO enhanced and suppressed days is shown by month for our study period from 1985 to 2019. The total number of suppressed MJO days per month varies between 161 (March) and 218 (January). For the enhanced phase, the numbers range from 110 days (December) to 203 days (March).

#### 4.2. Influence of the MJO on the diurnal cycles of convection and rainfall

The diurnal cycles of CCF and the GDI, indicating deep convection, are shown in Fig. 2a and b for the MJO enhanced convective (blue) and suppressed convective (red) phases as well as the climatology (black). Convection peaks in the afternoon, followed by a decrease in clouds during the night and a minimum in the morning, where the CCF and GDI values are generally higher during the MJO enhanced phase and lower during the suppressed phase, as would be expected. According to the purple line representing the RMD between the two MJO phases (right y-axis), the difference is lowest in the afternoon (0.2 for the CCF and 0.093 for the GDI) and increases during the nighttime until it peaks at 09:00 UTC for the CCF (0.65) and at 07:00 UTC for the GDI (0.123). The small difference in timing between the CCF and the GDI could be the result of the fact that the GDI was developed for the operational analysis and forecasting of tropical convection, and the atmosphere is evaluated before convection occurs, where radiative and evaporative cooling induced by clouds will weaken the GDI. Therefore, the GDI is showing

the highest values right before peak convection.

In addition to the analysis of MJO induced changes on cold clouds (i.e., CCF), the impacts of the MJO on warmer cloud fractions were investigated next, where Fig. 2c and d show the diurnal cycles of cloud fractions with  $T_b$  between  $-50\text{ }^\circ\text{C}$  and  $-25\text{ }^\circ\text{C}$  (Fig. 2c), and  $-25\text{ }^\circ\text{C}$  and  $0\text{ }^\circ\text{C}$  (Fig. 2d) for both MJO phases. The cloud fraction with  $T_b$  between  $-50\text{ }^\circ\text{C}$  and  $-25\text{ }^\circ\text{C}$  peaks at 21:00 UTC during the suppressed phase and at 00:00 UTC during the enhanced phase, indicating a slightly delayed peak during the enhanced phase. A minimum is recorded at 09:00 UTC for both phases. For the cloud fractions with  $T_b$  between  $-25\text{ }^\circ\text{C}$  and  $0\text{ }^\circ\text{C}$ , the maximum is slightly later at 03:00 UTC while the minimum is shown at 15:00 UTC for both phases. The RMDs between the enhanced and suppressed MJO phase are significant ( $p < 0.05$ ) at all times for both cloud fractions, where the difference is highest at 09:00 UTC for the colder cloud fraction and at 12:00 UTC for the warmer fraction. These consistently and significantly higher fractions of clouds with cloud top temperatures higher than  $-50\text{ }^\circ\text{C}$  during the MJO enhanced phase suggest that the MJO not only affects very cold clouds (i.e., CCF in Fig. 2a) but also greatly impacts warmer clouds.

In Fig. 3a and b, the impacts of the MJO on TRMM and ERA5 precipitation are analyzed, showing a peak in precipitation in the afternoon at 15:00 UTC for the TRMM and at 14:00 UTC for the ERA5 data, where precipitation amounts are generally higher for the ERA5 when compared to the TRMM data. A morning minimum is recorded at 09:00 UTC for TRMM, and at 06:00 UTC for the ERA5 data, which is consistent with the diurnal variations of the CCF and the GDI. As expected, the amount of precipitation is generally higher during the MJO enhanced phase, where the RMD between the two MJO phases is highest through the nighttime and the early morning for both datasets, with the difference peaking at 09:00 UTC for TRMM and at 07:00 UTC for ERA5, similar to the timing of the RMD of CCF and the GDI. Thus, the largest differences in precipitation and convective clouds between both MJO

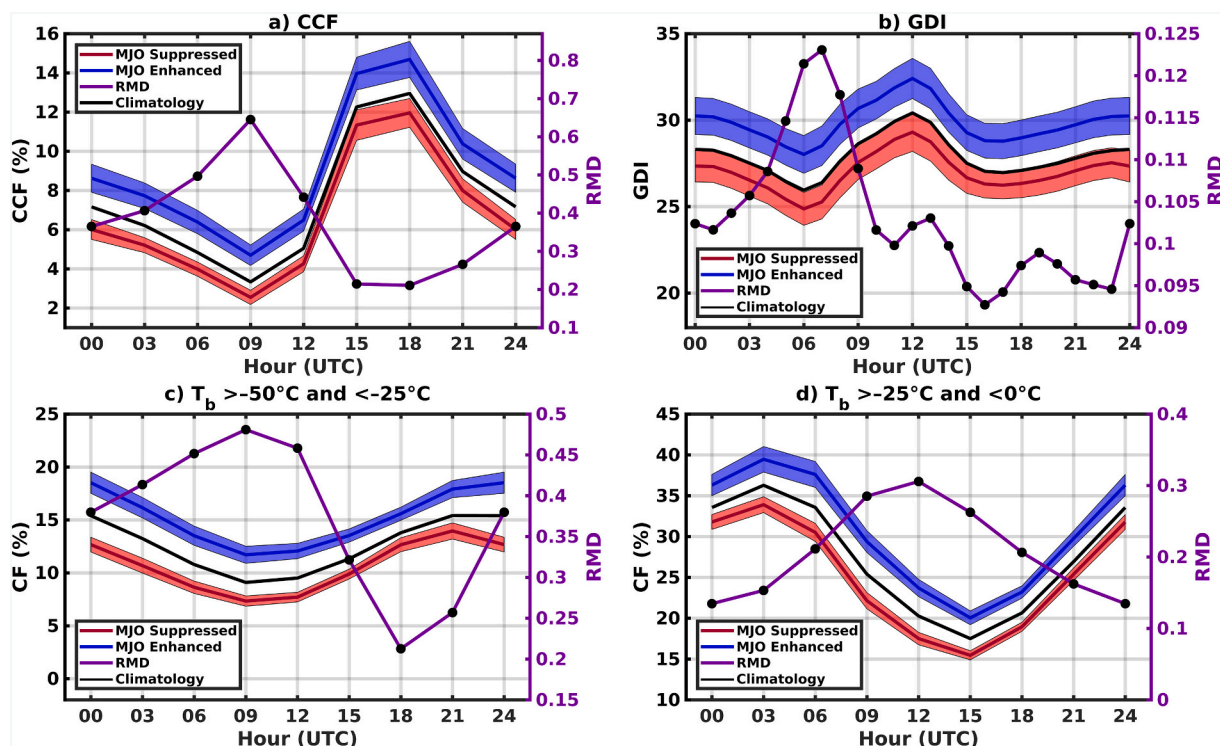
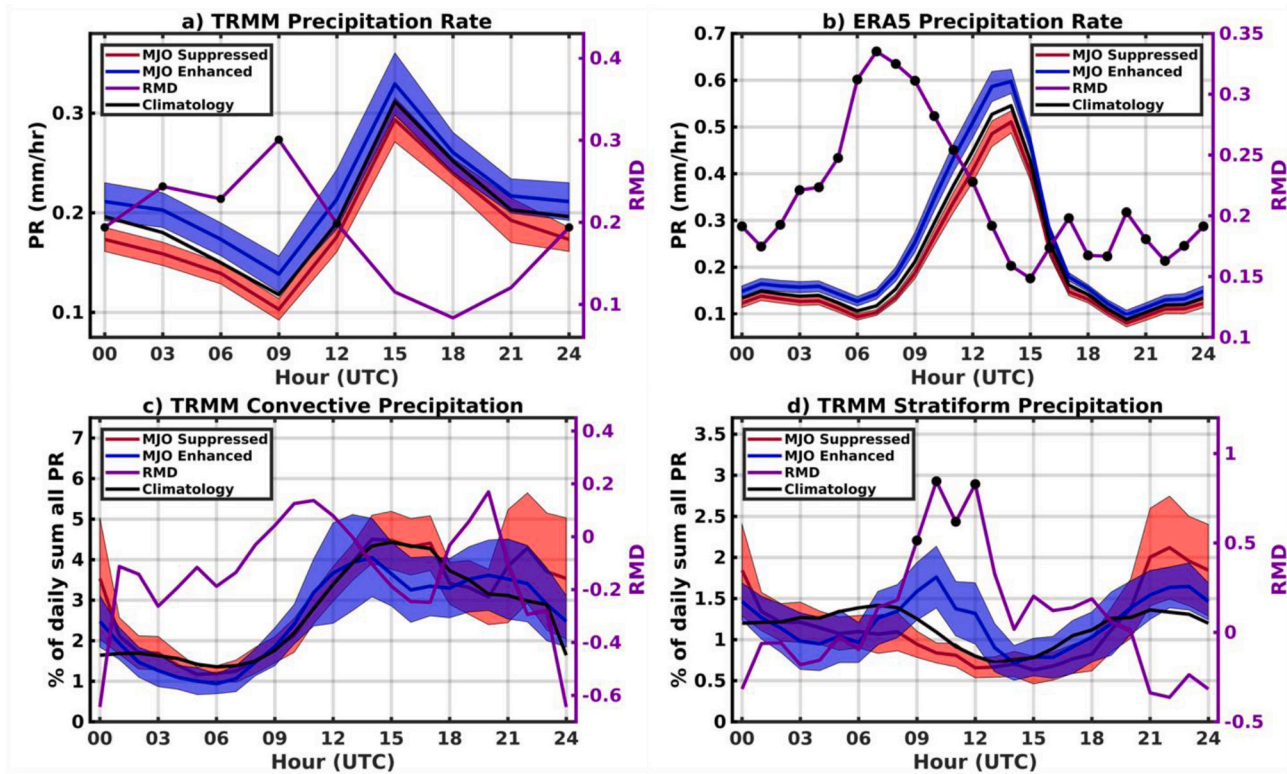


Fig. 2. Diurnal cycles of (a) GridSat-B1 CCF, (b) ERA5 GDI, (c) GridSat-B1 cloud fractions with  $T_b$  between  $-50\text{ }^\circ\text{C}$  and  $-25\text{ }^\circ\text{C}$ , and (d) GridSat-B1 cloud fractions with  $T_b$  between  $-25\text{ }^\circ\text{C}$  and  $0\text{ }^\circ\text{C}$  averaged over the study region from 1985 to 2019. The red line shows the distribution for the MJO suppressed phase, the blue line shows the distribution for the MJO enhanced phase, the black line indicates the climatology, and the purple line represents the RMD between the enhanced and suppressed phase (right y-axis). The 95% confidence intervals are indicated by the blue and red shadings. The black dots indicate that the difference is significant at  $p < 0.05$ . (For interpretation of the references to colour in this figure legend, the reader is referred to the web version of this article.)



**Fig. 3.** Diurnal cycles of (a) TRMM precipitation (1998–2019), (b) ERA5 precipitation (1985–2019), (c) TRMM convective precipitation contributions to the daily sum (1998–2013), and (d) TRMM stratiform precipitation contributions to the daily sum (1998–2013), averaged over the study region. The red line represents the distribution for the MJO suppressed phase, the blue line shows the distribution for the MJO enhanced phase, the black line indicates the climatology, and the purple line represents the RMD between the enhanced and suppressed phase (right y-axis). The black dots indicate that the difference is significant at  $p < 0.05$ . A 4-h smoothing was applied to the data TRMM convective and stratiform precipitation data due to the high spatial variability of the TRMM 2A23 sampling. (For interpretation of the references to colour in this figure legend, the reader is referred to the web version of this article.)

phases seem to occur during the nighttime and morning, when convective processes weaken. During this dissipating stage, the anvil cloud reaches maximal horizontal extent and begins to weaken, while the optical thickness of the cloud decreases, cloud top temperatures begin to increase, and the precipitation changes from convective to more stratiform. Therefore, the impacts of the MJO on stratiform and convective precipitation were investigated separately in a next step, where Fig. 3c and d show the diurnal cycles of convective (Fig. 3c) and stratiform (Fig. 3d) precipitation for the MJO enhanced and suppressed phases. The convective and stratiform precipitation is indicated as fractions of the daily sum of all precipitation, where 59.6% of all precipitation was classified as convective, 36.3% was classified as stratiform, and 4.1% was classified as other. Please note that the TRMM convective and stratiform precipitation data is available from 1998 to 2013 only, while the TRMM total precipitation is available from 1998 to 2019. Although the years 1998 to 2019 were used in this study for the TRMM total precipitation, the diurnal cycle of total precipitation is similar when using the timespan 1998 to 2013 only.

The convective precipitation fractions for the MJO enhanced and suppressed phases are similar, where a minimum is recorded at around 06:00 UTC for both MJO phases. For the enhanced phase, a first maximum occurs around 14:00 UTC (4.0%) with a second smaller peak at 20:00 UTC (3.6%). During the suppressed phase, a first maximum is recorded around 14:00 UTC (4.5%), followed by a second peak at 22:00 UTC (4.3%). The stratiform precipitation fraction exhibits a minimum at 14:00 UTC during the enhanced phase (0.7%) and 15:00 UTC during the suppressed phase (0.6%), followed by an increase in precipitation with a maximum at 22:00 UTC during the suppressed phase (2.1%). For the enhanced MJO phase, a first maximum is recorded at 23:00 UTC (1.6%),

followed by a second peak at 10:00 UTC (1.7%). The difference between the two phases is highest at that time, where the difference is significant ( $p < 0.05$ ) between 09:00 and 12:00 UTC. These results suggest that the difference in precipitation between the MJO enhanced and suppressed phase shown in Fig. 3a is mainly due to the difference in the stratiform precipitation. Thus, the MJO may impact the stratiform precipitation more than convective precipitation.

#### 4.3. Possible physical mechanisms responsible for the MJO induced modulations

To investigate the underlying physical processes leading to the observed differences in the diurnal cycles of precipitation and convection between the MJO enhanced and suppressed phases, two variables relevant to vertical circulation, i.e., horizontal divergence and vertical velocity, were investigated next (Fig. 4). Divergence and vertical velocity profiles are useful to gain information about heating profiles since they are tightly coupled and play an important role in large-scale tropical dynamics (Mapes and Lin, 2005). The vertical and diurnal structures of divergence shown in Fig. 4a and c are similar for both MJO phases. For the upper tropospheric levels (100 hPa to 300 hPa), divergence is prominent during all hours of the day with the strongest values in the evening. From 300 hPa to 400 hPa, a band of convergent air motion is recorded. In the mid-levels from 400 hPa to 700 hPa, divergent air motion is evident from the nighttime through the early afternoon, where divergence is strongest between 08:00 UTC and 12:00 UTC. During the afternoon and evening, the airflow changes from divergent to convergent. In the levels below 700 hPa, the airflow is convergent during all times of day. The contour lines show that the biggest anomalies are



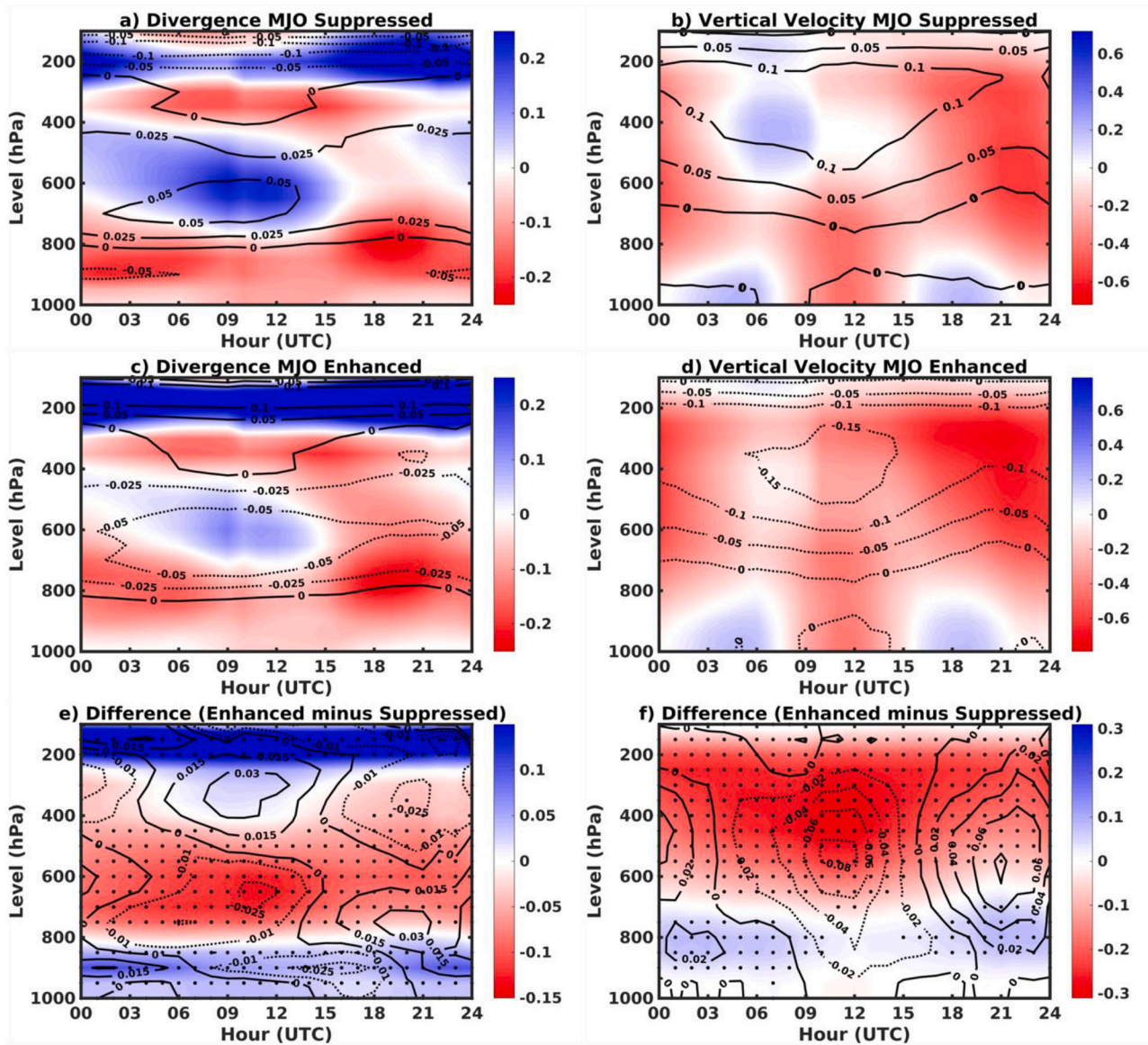


**Fig. 4.** (a–d): Time–height cross sections of (a), (c) ERA5 divergence ( $10^{-5} \times \text{s}^{-1}$ ) and (b), (d) ERA5 vertical velocity ( $10^{-1} \times \text{Pa s}^{-1}$ ) for the MJO suppressed phase (top) and the MJO enhanced phase (middle), averaged over the study region from 1985 to 2019. The shading represents the values averaged over all MJO suppressed days and all MJO enhanced days, respectively. The black contour lines indicate the anomalies (i.e., the difference between the MJO enhanced/suppressed days and all days during ONDJFM). (e–f): Difference between the MJO enhanced and suppressed phase for (e) ERA5 divergence and (f) ERA5 vertical velocity (shading) where the black dots indicate that the difference is significant at  $p < 0.05$ . The contour lines show the diurnal variations of the difference.

recorded in the upper levels during all times of day and during the morning hours in the mid-levels, where divergence is anomalously strong in the mid-levels during the suppressed phase and in the upper levels during the enhanced phase.

Looking at the time–height cross sections of vertical velocity (Fig. 4b and d), the diurnal patterns are similar during both MJO phases as well. The figures indicate evening and nighttime subsidence in the lowest levels (900 hPa to 1000 hPa), uplift in the low and mid-levels (600 hPa to 1000 hPa) from the late morning through the early afternoon, and strong rising motion during the afternoon and evening from the mid through the upper levels (200 hPa to 700 hPa). Additionally, there is subsidence evident during the suppressed phase from 100 hPa to 500 hPa from around 03:00 to 10:00 UTC, while the air motion is neutral or lightly upward during the enhanced phase at the same time and levels, besides a small area of subsidence at 100 hPa. This may lead to shallower convection and faster dissipation of the stratiform precipitation portions of the clouds during the suppressed phase. According to the contour

lines, the largest anomalies for both phases are occurring around 400 hPa in the morning and early afternoon hours.

Although the vertical and diurnal divergence and vertical velocity structures are similar during the MJO enhanced and suppressed phase, important differences between the two phases can be observed, mostly related to the strength of the airflow, where Fig. 4e and f highlight those differences. Fig. 4e shows stronger upper-level divergence during all times of the day and weaker mid-level divergence at night during the MJO enhanced phase. Additionally, mid-level convergence is stronger in the afternoon and evening during the enhanced phase. These results suggest deeper convection and stronger stratiform precipitation portions of deep convection when the MJO is in its enhanced phase. The contour lines in Fig. 4e show variation from the diurnal average of the anomalies at each level and hour, highlighting the diurnal variations of the differences between the two MJO phases. For the upper levels, the variations are greatest from 03:00 UTC to 05:00 UTC, indicating that the differences are greatest during the nighttime. For the mid-levels, the

differences are enhanced from around 09:00 UTC to 13:00 UTC, and for the lower levels, they are strongest from 00:00 UTC to 03:00 UTC. Overall, the differences in divergence between the two MJO phases are largest in the upper levels, followed by the mid and lower levels. In the upper and lower levels, the differences are strongest during the nighttime. For the mid-levels, the differences are largest during the mid-morning, which is consistent with the time of peak changes in convection and precipitation shown in Figs. 2 and 3.

For the vertical velocity, the difference cross section (Fig. 4f) shows that there is generally more upward air motion during the enhanced phase from 100 hPa to around 700 hPa during all times of day, where the difference is most pronounced from about 09:00 UTC to 13:00 UTC. To a smaller extent, there is more subsidence during the enhanced phase in the lower levels. As shown by the contour lines indicating the variations across the day, the difference between the two MJO phases is largest from 09:00 UTC to 13:00 UTC from 400 hPa to 600 hPa, which is consistent with the time of the largest differences in precipitation and convection shown in Fig. 2. In the levels below 700 hPa, the largest differences are recorded from the evening through the early morning.

In summary, upward air motion is stronger during the MJO enhanced phase when compared to the suppressed phase, especially in the mid-levels and around noon. Additionally, upper-level divergence is stronger during the MJO enhanced phase. During the suppressed phase, nighttime and morning mid- and upper-level subsidence and mid-level divergence are pronounced. Regarding the diurnal variations, the largest differences in divergence and vertical velocity between the two MJO phases occur from the late morning through the early afternoon in the mid-levels which is consistent with the time of the largest differences in precipitation and convection, and during the nighttime in the lower

(divergence and vertical velocity) and upper (divergence only) levels. Furthermore, the timing of peak TRMM and ERA5 precipitation and GridSat-B1 CCF is consistent with the strong upward vertical velocities as well as enhanced convergence in the low- and mid-levels and strong divergence in the upper levels derived from the ERA5 data, indicating that the two satellite datasets are generally consistent with the ERA5 reanalysis data.

To better explain the different impacts of the MJO on stratiform and convective precipitation, the time-height cross sections for wind speed, relative humidity, and temperature are shown in Fig. 5 since previous studies (e.g., Schumacher and Houze Jr., 2003; Schumacher and Houze, 2006; Lin et al., 2004) suggest that wind shear and relative humidity play an important role in the formation of stratiform precipitation, and deep convection may also impact the temperature in the troposphere (Johnston et al., 2018). The diurnal wind speed patterns are relatively similar during both MJO phases (Fig. 5a and d). However, the diurnal structures are generally weaker during the enhanced phase. The contour lines, indicating the anomalies during the respective MJO phase, show the largest anomalies in the upper levels during both phases. Additionally, Fig. 5g shows that wind speeds are generally weaker in the mid-levels and stronger in the upper and lower levels during the enhanced phase. This may contribute to the increased production of stratiform precipitation during the enhanced phase since weaker mid-level winds may increase stratiform rain by decreasing entrainment in stratiform clouds through decreased sublimation and evaporation (Schumacher and Houze, 2006). Furthermore, vertical wind shear appears to be stronger during the enhanced phase, which contributes to convective organization (Anber et al., 2014; Robe and Emanuel, 2001) and may also increase stratiform precipitation (Saxen and Rutledge, 2000). The

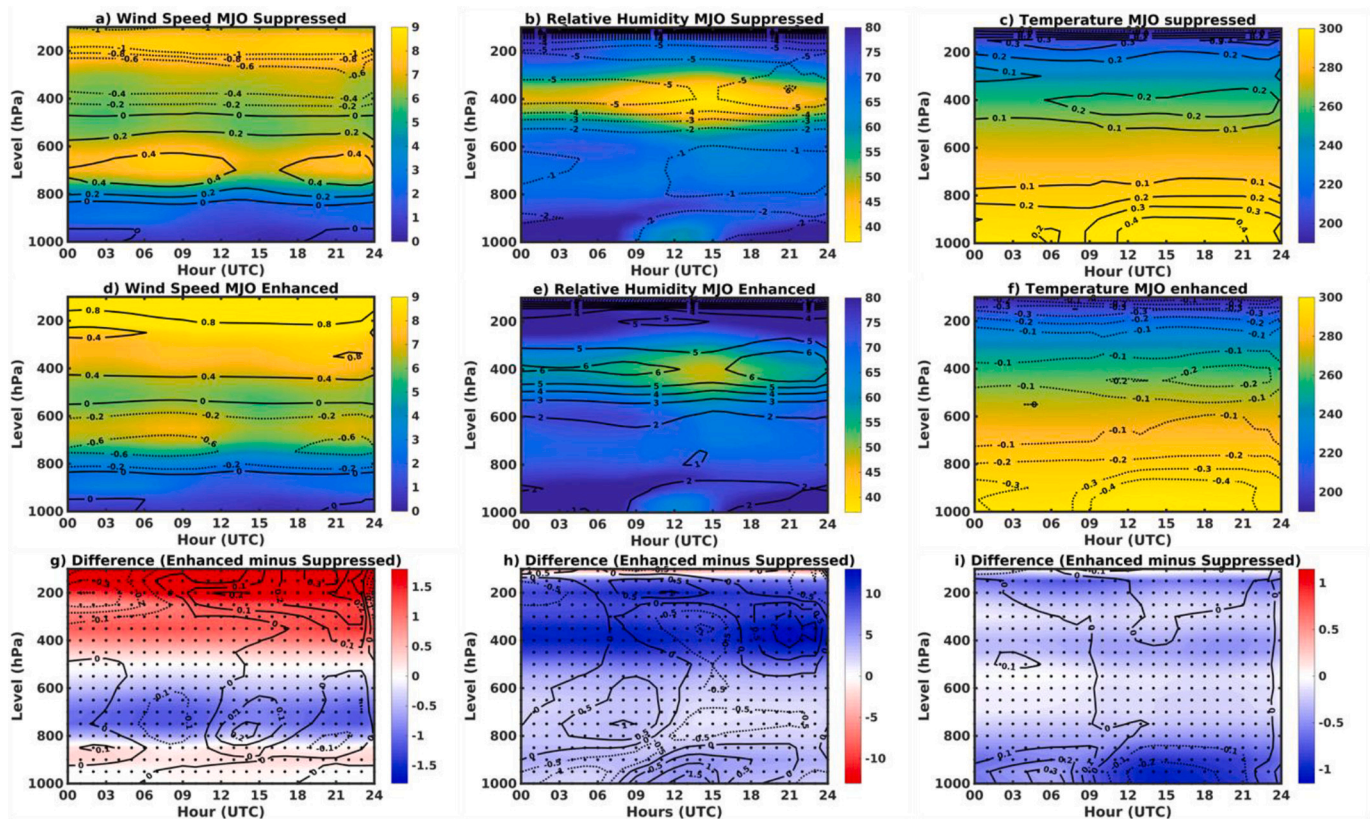


Fig. 5. (a–f) Time-height cross section of (a), (d) ERA5 wind speed ( $\text{ms}^{-1}$ ), (b), (e) ERA5 relative humidity (%), and (c), (f) ERA5 temperature (K) for the MJO suppressed phase (top) and the MJO enhanced phase (middle), averaged over the study region from 1985 to 2019. The shading represents the values averaged over all MJO suppressed days and all MJO enhanced days, respectively. The black contour lines indicate the anomalies (i.e., the difference between the MJO enhanced/suppressed days and all days during ONDJFM). (g–i): Difference between the MJO enhanced and suppressed phase for (g) ERA5 wind speed, (h) ERA5 relative humidity, and (i) ERA5 temperature (shading) where the black dots indicate that the difference is significant at  $p < 0.05$ . The contour lines show the diurnal variations of the difference.



diurnal variations of the differences between the two MJO phases (contour lines in Fig. 5g) are relatively small, where the highest differences are recorded from 18:00 UTC to 21:00 UTC in the upper levels, from 05:00 UTC to 10:00 UTC in the mid-levels, and from 00:00 UTC to 05:00 UTC in the lowest levels. The observed decrease in wind speed in the mid-levels during the enhanced phase, which is most pronounced during the mornings, might be another contributing factor to the increased stratiform precipitation during the morning.

The relative humidity profiles (Fig. 5b, e, and h) show generally higher relative humidity during the enhanced phase. The contour lines in Fig. 5b and e, as well as the shading in Fig. 5h indicate that the differences between the two MJO phases are greatest around 400 hPa. Similar to the wind speed, the diurnal structures of relative humidity are weakened during the enhanced phase, where the area of lower relative humidity around 400 hPa is less pronounced during the enhanced phase. According to the contour lines in Fig. 5h indicating the diurnal variations of the difference, the highest differences are recorded in the evening from 100 hPa to 600 hPa, from 03:00 UTC to 10:00 UTC from 600 hPa to 800 hPa, and from 12:00 UTC to 15:00 UTC from 800 hPa to 1000 hPa. Thus, the higher relative humidity during the MJO enhanced phase, especially in the upper and mid-levels during the nighttime and morning, may help in enhancing precipitation during the MJO enhanced phase. The observed higher relative humidity during the enhanced phase may also be contributing to the observed increase in stratiform precipitation during that phase, since studies such as Schumacher and Houze (2006) propose that a moist atmosphere may assist stratiform growth.

The temperature profiles (Fig. 5c and f) show similar structures overall, with generally colder temperatures during the MJO enhanced phase where the greatest differences are recorded in the afternoon and early evening below 800 hPa (Fig. 5i). Increased deep convection during the MJO enhanced phase could possibly be leading to enhanced atmospheric cooling and cold convective downdrafts, resulting in a transport of cold air to the lower levels and subsequently lowering the air temperature near the surface. Additionally, evaporative and radiative cooling could also be contributing factors to the lower temperatures during the MJO enhanced phase (Schiro and Neelin, 2018; Rooney et al., 2018).

Overall, the higher relative humidity and the lower wind speed in the mid-levels in the morning during the enhanced phase could both be factors contributing to the development of increased stratiform precipitation in the morning with convective cooling possibly leading to the observed lower temperatures during the enhanced phase.

## 5. Summary and discussion

This study analyzes the impacts of the MJO on the diurnal cycles of convection and precipitation from 1985 to 2019, using TRMM and GridSat-B1 satellite as well as ERA5 reanalysis data. Additionally, the physical mechanisms leading to the observed differences in the diurnal cycles between the MJO enhanced and suppressed phases are investigated using ERA5 vertical velocity, divergence, wind speed, relative humidity, and temperature data. Results show that the differences between the MJO enhanced and suppressed phases are largest during the nighttime and morning hours when convection is weakest and are possibly the result of circulation changes due to the MJO. Fig. 6 summarizes the most important processes observed during the MJO enhanced and suppressed convective phase, respectively, and highlights the differences in clouds, precipitation, horizontal divergence, and vertical velocity between the two MJO phases, where the green arrows indicate the processes that are most important for the respective MJO phase compared to the other phase. During the MJO suppressed phase (Fig. 6a), subsidence is evident in the upper and mid-levels during the nighttime and morning hours (Fig. 4b), accompanied by strong divergence in the mid-levels (Fig. 4a). The observed subsidence and divergence may suppress convection, enhance the decay of convective clouds and the dissipation of the anvil while also inhibiting the vertical growth of new convective cores and vertical updrafts in the mid and upper levels. This will eventually result in more shallow convection and weakened stratiform precipitation portions of deep convection, ultimately leading to a decrease in stratiform precipitation (Fig. 3). During the enhanced phase (Fig. 6b), divergence in the upper levels is stronger, while nighttime and morning divergence in the mid-levels is much weaker (Fig. 4c). The air motion is generally upward with no observed subsidence in the mid- and upper levels (Fig. 4d), which may lead to the weaker mid-level divergence. This is possibly causing a slower decay of older convective clouds and dissipation of anvils during the nighttime and morning, and may encourage the growth of new convective cores, resulting in larger anvils and enhanced stratiform precipitation rates (Fig. 3). Additionally, mid-level rising air motions and convergence are enhanced in the afternoon and evening (Fig. 4d), which is possibly contributing to the increased and deeper afternoon convection as well as the increased precipitation amounts.

The above-described observed impacts of the MJO on the diurnal cycles of precipitation and convection over the Congo differ somewhat from the MJO's influence on other tropical regions close to the MJO's center. Oh et al. (2012) analyzed the impacts of the MJO on the diurnal cycle of rainfall over the western MC and found the largest impacts over land to occur during peak convection in the afternoon and not during the

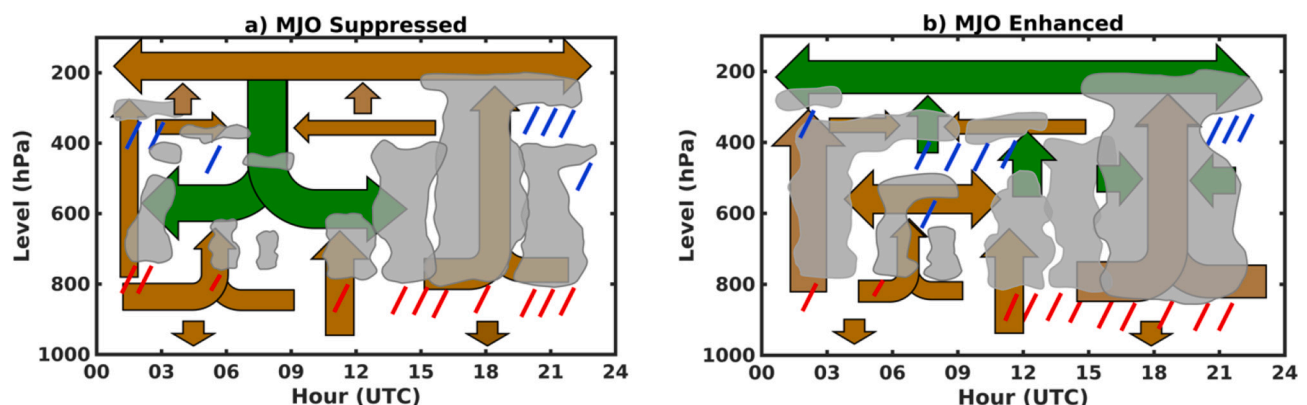


Fig. 6. Schematic of the diurnal cycle for the (a) MJO suppressed and (b) MJO enhanced phase, for clouds, rainfall, and air motions (i.e., divergence and vertical motions), where the green colored arrows indicate dominant processes during the respective MJO phase compared to the other MJO phase, and the brown arrows indicate less important processes for the respective phase. Convective precipitation is indicated by the red lines at the bottom of the convective clouds and stratiform precipitation is represented by the blue lines at the anvils. (For interpretation of the references to colour in this figure legend, the reader is referred to the web version of this article.)

morning, showing an increased hourly maximum rain rate during the MJO enhanced phase when compared to the suppressed phase. The observed changes are attributed to anomalous low-level winds during the respective MJO phase, interacting with the monsoonal flow over the MC. Liu et al. (2022) also found the MJO to be interacting with the American and African monsoons through different mechanisms, for example by exciting Kelvin waves and mid-latitude teleconnections. While we found small changes in the diurnal amplitudes of precipitation or convection, Lu et al. (2019) showed that the difference between the MJO enhanced and suppressed phase over the MC mainly reveals itself in variations of the diurnal amplitude of precipitation, where the amplitude is larger during the enhanced phase and smaller during the suppressed phase. The differences are mainly attributed to changes in wind and moisture convergence and divergence patterns. Sakaeda et al. (2017) also observed a difference in the amplitude of the diurnal rainfall rates between both MJO phases over the MC, together with a delayed peak in rainfall during the MJO enhanced phase. Similar to our results, Sakaeda et al. (2017) also observed enhanced stratiform precipitation after peak convective rainfall during the enhanced phase, which might be causing the observed delay in peak rainfall. They conclude that convection is more organized during the MJO enhanced phase, leading to increased formation of stratiform anvil clouds with greater horizontal extents, which will contribute to increased total rainfall rates. The differences in the MJO's impacts over the Congo from other tropical regions such as the MC could be the result of differences in topography, where the MC consists of multiple islands of different sizes surrounded by the ocean, while the Congo basin sits in the center of the African continent containing dense tropical rainforest promoting intense convection, surrounded by land on three sides and the Atlantic Ocean in the west.

A limitation of this study is the usage of regional averaging over the entire study domain for the diurnal cycles and the atmospheric fields. This domain-wide averaging does not account for the fact that convection and precipitation varies spatially across the Congo basin and does not exclude grid-points which may not be raining. If including only the rainy points, for example during the enhanced phase, the specific divergence and vertical velocity patterns might be more pronounced when compared to including all grid points. Additionally, while this study discovers the impacts of the MJO on the diurnal cycles of convection and precipitation and explores some physical mechanisms leading to the observed changes, further work is needed to fully understand how the MJO modulates the diurnal variabilities of convection and rainfall. For example, explaining why the MJO is influencing the stratiform and convective precipitation differently could enhance our understanding about the MJO's impact on precipitation and may help to better resolve and simulate the MJO and associated variabilities in rainfall and convection, ultimately improving predictions of MJO modulated rainfall. Additional analysis on the impacts of the MJO on storm lifetime and initiation using high spatial and temporal resolutions data could also be useful to understand variations in the frequency, intensity, and duration of convective systems due to the MJO.

Overall, the results presented above answer the question of how the MJO, the most dominant intraseasonal variability in the tropics, impacts convection and precipitation over the Congo from a diurnal perspective and improve our understanding about factors influencing the diurnal cycle of convection and rainfall over tropical rainforests. Our findings are not only useful in identifying the main drivers of the observed long-term and large-scale drying trend that has been stressing the Congo Basin but also help in improving weather forecasts and model development. For example, one major finding of this study is that the impact of the MJO on convection and rainfall is greatest in the morning hours, influencing the stratiform portion of the rain more than the convective precipitation. Since the changes in rainfall and convection are largest during the morning hours when rainfall totals are usually lowest, the MJO could be used to predict exceptionally high precipitation rates in the morning. Additionally, considering that the MJO modulates

convective and stratiform precipitation differently could help to predict the modulation of rainfall by the MJO more accurately.

### CRediT authorship contribution statement

**Kathrin Alber:** Conceptualization, Methodology, Software, Validation, Formal analysis, Investigation, Data curation, Writing – original draft, Visualization. **Liming Zhou:** Conceptualization, Writing – review & editing, Funding acquisition. **Paul E. Roundy:** Conceptualization, Writing – review & editing. **Stephen L. Solimine:** Data curation, Writing – review & editing.

### Declaration of Competing Interest

The authors declare that they have no known competing financial interests or personal relationships that could have appeared to influence the work reported in this paper.

### Data availability

Data will be made available on request.

### Acknowledgements

This work is supported by the National Science Foundation (NSF AGS-1854486). We thank Dr. Ajay Raghavendra for the insightful discussions that contributed to this study and helped to improve the quality of the work.

### References

- Alaka, G.J., Maloney, E.D., 2012. The influence of the MJO on upstream precursors to African easterly waves. *J. Clim.* 25 (9), 3219–3236.
- Alber, K., Zhou, L., Raghavendra, A., 2021a. A shift in the diurnal timing and intensity of deep convection over the Congo Basin during the past 40 years. *Atmos. Res.* 264, 0169–8095.
- Alber, K., Raghavendra, A., Zhou, L., Jiang, Y., Sussman, H.S., Solimine, S.L., 2021b. Analyzing intensifying thunderstorms over the Congo Basin using the Gálvez-Davison index from 1983–2018. *Clim. Dyn.* 56, 949–967.
- Alsdorf, D., et al., 2016. Opportunities for hydrologic research in the Congo Basin. *Rev. Geophys.* 54, 378–409.
- Anber, U., Wang, S., Sobel, A.H., 2014. Response of atmospheric convection to vertical wind shear: cloud-system resolving simulations with parameterized large-scale circulation. Part I: specified radiative cooling. *J. Atmos. Sci.* 71, 2976–2993.
- Awaka, J., Iguchi, T., Kumagai, H., Okamoto, K., 1997. Rain type classification algorithm for TRMM precipitation radar. *J. Appl. Meteorol.* 42, 1633–1635. IEEE 1997 Int. Geoscience and Remote Sensing Symp., Singapore, Japan, Institute of Electrical and Electronics Engineers.
- Berhane, F., Zaitchik, B., 2014. Modulation of daily precipitation over East Africa by the Madden-Julian Oscillation. *J. Clim.* 27, 6016–6034.
- Dias, J., Sakaeda, N., Kiladis, G.N., Kikuchi, K., 2017. Influences of the MJO on the space-time organization of tropical convection. *J. Geophys. Res. Atmos.* 122, 8012–8032.
- Feng, Z., Leung, L.R., Liu, N., Wang, J., Houze Jr., R.A., Li, J., Hardin, J.C., Chen, D., Guo, J., 2021. A global high-resolution mesoscale convective system database using satellite-derived cloud tops, surface precipitation, and tracking. *J. Geophys. Res.-Atmos.* 126 (8) p.e2020JD034202.
- Gálvez, J.M., Davison, M., 2016. The Gálvez-Davison Index for Tropical Convection. [https://www.wpc.ncep.noaa.gov/international/gdi/GDI\\_Manuscript\\_V20161021.pdf](https://www.wpc.ncep.noaa.gov/international/gdi/GDI_Manuscript_V20161021.pdf). Accessed December 2022.
- Gleixner, S., Demissie, T., Diro, G.T., 2020. Did ERA5 improve temperature and precipitation reanalysis over East Africa? *Atmosphere* 2020 (11), 996.
- Gottschalck, J., Wheeler, M., Weickmann, K., Vitart, F., Savage, N., et al., 2010. A framework for assessing operational Madden-Julian oscillation forecasts: a CLIVAR MJO working group project. *Bull. Am. Meteorol. Soc.* 91, 1247–1258.
- Hart, N.C., Reason, C.J., Fauchereau, N., 2013. Cloud bands over southern Africa: Seasonality, contribution to rainfall variability and modulation by the MJO. *Clim. Dyn.* 41, 1199–1212.
- Hart, N.C., Washington, R., Maidment, R.I., 2019. Deep convection over Africa: annual cycle, ENSO, and trends in the hotspots. *J. Clim.* 32, 8791–8811.
- Hartman, A.T., 2021. Tracking mesoscale convective systems in central equatorial Africa. *Int. J. Climatol.* 41 (1), 469–482.
- Hendon, H.H., Woodberry, K., 1993. The diurnal cycle of tropical convection. *J. Geophys. Res.* 98, 16 523–16 637.
- Hersbach, H., et al., 2020. The ERA5 global reanalysis Q. *J. R. Meteorol. Soc.* 1–51.
- Houze Jr., R.A., 1997. Stratiform precipitation in regions of convection: a meteorological paradox? *Bull. Am. Meteor. Soc.* 78, 2179–2196.



- Hua, W., Zhou, L., Chen, H., Nicholson, S.E., Jiang, Y., Raghavendra, A., 2016. Possible causes of the Central Equatorial African long-term drought. *Environ. Res. Lett.* 11, 124002.
- Hua, W., Zhou, L., Chen, H., Nicholson, S.E., Jiang, Y., Raghavendra, A., 2018. Understanding the Central Equatorial African long-term drought using AMIP-type simulations. *Clim. Dyn.* 50, 1115–1128.
- Hua, W., Zhou, L., Nicholson, S.E., Chen, H., Qin, M., 2019. Assessing reanalysis data for understanding rainfall climatology and variability over Central Equatorial Africa. *Clim. Dyn.* 53, 651–669.
- Huffman, G.J., Bolvin, D.T., Nelkin, E.J., Wolff, D.B., Adler, R.F., Gu, G., Hong, Y., Bowman, K.P., Stocker, E.F., 2007. The TRMM multisatellite precipitation analysis (TMPA): quasi-global, multiyear, combined-sensor precipitation estimates at fine scales. *J. Hydrometeorol.* 8, 38–55.
- Jackson, B., Nicholson, S.E., Klotter, D., 2009. Mesoscale convective systems over western equatorial Africa and their relationship to large-scale circulation. *Mon. Weather Rev.* 137, 1272–1294.
- Jiang, Y., Zhou, L., Tucker, C.J., Raghavendra, A., Hua, W., Liu, Y., Joiner, J., 2019. Widespread increase of boreal summer dry season length over the Congo rainforest. *Nat. Clim. Chang.* 9, 617–622.
- Jiang, Y., Zhou, L., Roundy, P.E., Hua, W., Raghavendra, A., 2021. Increasing influence of Indian Ocean dipole on precipitation over Central Equatorial Africa. *Geophys. Res. Lett.* 48 e2020GL02370.
- Johnston, B.R., Xie, F., Liu, C., 2018. The effects of deep convection on regional temperature structure in the tropical upper troposphere and lower stratosphere. *J. Geophys. Res. Atmos.* 123, 1585–1603.
- Kim, H.M., Webster, P.J., Hoyos, C.D., Kang, I.-S., 2008. Sensitivity of MJO simulation and predictability to sea surface temperature variability. *J. Clim.* 21, 5304–5317.
- Knapp, K.R., 2008. Scientific data stewardship of International Satellite Cloud Climatology project B1 global geostationary observations. *J. Appl. Remote. Sens.* 2, 023548.
- Knapp, K.R., et al., 2011. Globally gridded satellite observations for climate studies. *Bull. Am. Meteorol. Soc.* 92, 893–907.
- Lazri, M., Ameur, S., Brucker, J.M., Ouallouche, F., 2014. Convective rainfall estimation from MSG/SEVIRI data based on different development phase duration of convective systems (growth phase and decay phase). *Atmos. Res.* 147–148, 38–50.
- Lin, J., Mapes, B.E., Zhang, M., Newman, M., 2004. Stratiform precipitation, vertical heating profiles, and the Madden-Julian Oscillation. *J. Atmos. Sci.* 61, 296–309.
- Liu, F., Wang, B., Ouyang, Y., et al., 2022. Intraseasonal variability of global land monsoon precipitation and its recent trend. *npj Clim. Atmos. Sci.* 5, 30.
- Lu, J., Li, T., Wang, L., 2019. Precipitation diurnal cycle over the Maritime Continent modulated by the MJO. *Clim. Dyn.* 53, 6489–6501.
- Madden, R.A., Julian, P.R., 1971. Detection of a 40–50 day oscillation in the zonal wind in the tropical Pacific. *J. Atmos. Sci.* 28, 702–708.
- Madden, R.A., Julian, P.R., 1972. Description of global-scale circulation cells in the tropics with a 40–50 day period. *J. Atmos. Sci.* 29, 1109–1123.
- Mapes, B.E., Lin, J., 2005. Doppler radar observations of mesoscale wind divergences in regions of tropical convection. *Mon. Weather Rev.* 133, 1808–1824.
- Maybee, B., Ward, N., Hirons, L.C., Marsham, J.H., 2022. Importance of Madden-Julian oscillation phase to the interannual variability of East African rainfall. *Atmos. Sci. Lett.* e1148.
- Miller, et al., 2019. An empirical study of the relationship between seasonal precipitation and thermodynamic environment in Puerto Rico. *Weather Forecast.* 34, 277–288.
- Munzimi, Y., Hansen, M., Adusei, B., Senay, G., 2015. Characterizing Congo Basin rainfall and climate using TRMM satellite data and limited rain gauge ground observations. *J. Appl. Meteorol. Climatol.* 54, 541–556.
- Negri, A.J., Bell, T.L., Xu, L., 2002. Sampling of the diurnal cycle of precipitation using TRMM. *J. Atmos. Ocean. Technol.* 19, 1333–1344.
- Nesbitt, S.W., Zipser, E.J., 2003. The diurnal cycle of rainfall and convective intensity to three years of TRMM measurements. *J. Clim.* 16, 1456–1475.
- Nicholson, S.E., 2018. The ITCZ and the seasonal cycle over equatorial Africa. *Bull. Am. Meteorol. Soc.* 30, 337–348.
- Nicholson, S.E., Klotter, D., Zhou, L., Hua, W., 2019. Validation of satellite precipitation estimates over the Congo Basin. *J. Hydrometeorol.* 20, 631–656.
- Oh, J.-H., Kim, K.-Y., Lim, G.-H., 2012. Impact of MJO on the diurnal cycle of rainfall over the western Maritime Continent in the austral summer. *Clim. Dyn.* 38, 1167–1180.
- Otto, F.E.L., Jones, R.G., Halladay, K., Allen, M.R., 2013. Attribution of changes in precipitation patterns in African rainforests. *Philos. Trans. R. Soc. B* 368 (1625), 20120299.
- Pohl, B., Camberlin, P., 2006. Influence of the Madden-Julian Oscillation on East African rainfall. I: intraseasonal variability and regional dependency. *Q. J. R. Meteorol. Soc.* 132, 2521–2539.
- Raghavendra, A., Zhou, L., Jiang, Y., Hua, W., 2018. Increasing extent and intensity of thunderstorms observed over the Congo Basin from 1982 to 2016. *Atmos. Res.* 213, 17–26.
- Raghavendra, A., Zhou, L., Roundy, P.E., et al., 2020. The MJO's impact on rainfall trends over the Congo rainforest. *Clim. Dyn.* 54, 2683–2695.
- Rauniyar, S.P., Walsh, K.J.E., 2011. Scale interaction of the diurnal cycle of rainfall over the Maritime Continent and Australia: influence of the MJO. *J. Clim.* 24, 325–348.
- Robe, F.R., Emanuel, K.A., 2001. The effect of vertical wind shear on radiative-convective equilibrium states. *J. Atmos. Sci.* 58, 1427–1445.
- Rooney, G.G., Van Lipzig, N.P.M., Thiery, W., 2018. Estimating the effect of rainfall on the surface temperature of a tropical lake. *Hydrol. Earth Syst. Sci.* 22, 6357–6369.
- Sakaeda, N., Kiladis, G., Dias, J., 2017. The diurnal cycle of tropical cloudiness and rainfall associated with the Madden-Julian oscillation. *J. Clim.* 30, 3999–4020.
- Saxen, T.R., Rutledge, S.A., 2000. Surface rainfall-cold cloud fractional coverage relationship in TOGA COARE: A function of vertical wind shear. *Mon. Wea. Rev.* 128, 407–415.
- Schiffer, R.A., Rossow, W.B., 1983. The International Satellite Cloud Climatology Project (ISCCP): the first project of the World Climate Research Program. *Bull. Am. Meteorol. Soc.* 64, 779–784.
- Shiro, K.A., Neelin, J.D., 2018. Tropical continental downdraft characteristics: Mesoscale systems versus unorganized convection. *Atmos. Chem. Phys.* 18, 1997–2010.
- Schumacher, C., Houze, R.A., 2006. Stratiform precipitation production over sub-Saharan Africa and the tropical East Atlantic as observed by TRMM. *Q. J. R. Meteorol. Soc.* 132 (620), 2235–2255.
- Schumacher, C., Houze Jr., R.A., 2003. Stratiform rain in the tropics as seen by the TRMM precipitation radar. *J. Clim.* 16, 1739–1756.
- Slingo, J., Inness, P., Neale, P., Woolnough, S., Yang, G.Y., 2003. Scale interactions on diurnal to seasonal timescales and their relevance to model systematic errors. *Ann. Geophys.* 46, 139–155.
- Sossa, A., Liebmann, B., Bladé, I., Allured, D., Hendon, H.H., Peterson, P., Hoell, A., 2017. Statistical connection between the Madden-Julian oscillation and large daily precipitation events in West Africa. *J. Clim.* 30 (6), 1999–2010.
- Sui, C.-H., Lau, K.-M., 1992. Multiscale phenomena in the tropical atmosphere over the western Pacific. *Mon. Weather Rev.* 120, 407–430.
- Sui, C.-H., Lau, K.-M., Takayabu, Y.N., Short, D.A., 1997. Diurnal variations in tropical oceanic cumulus convection during TOGA COARE. *J. Atmos. Sci.* 54, 639–655.
- Suzuki, T., 2009. Diurnal cycle of deep convection in super clusters embedded in the Madden-Julian oscillation. *J. Geophys. Res.* 114, D22102.
- Talib, J., Taylor, C.M., Harris, B.L., Wainwright, C.M., 2023. Surface-driven amplification of MJO circulation anomalies across East Africa and its influence on the Turkana jet. *Q. J. R. Meteorol. Soc.* 149, 1890–1912.
- Taylor, C.M., Belusic, D., Guichard, F., Parker, D.J., Vissel, T., Bock, O., Harris, P.H., Janicot, S., Klein, C., Panthou, G., 2017. Frequency of extreme Sahelian storms tripled since 1982 in satellite observations. *Nature* 544, 475–478.
- Taylor, C.M., Fink, A.H., Klein, C., Parker, D.J., Guichard, F., Harris, P.P., Knapp, K.R., 2018. Earlier seasonal onset of intense mesoscale convective systems in the Congo Basin since 1999. *Geophys. Res. Lett.* 45 (24), 13–458.
- Tian, B.J., Waliser, D.E., Fetzner, 2006. Modulation of the diurnal cycle of tropical deep convective clouds by the MJO. *Geophys. Res. Lett.* 33, L20704.
- Vashisht, A., Zaitchik, B., 2022. Modulation of East African boreal fall rainfall: combined effects of the Madden-Julian oscillation (MJO) and El Niño–Southern oscillation (ENSO). *J. Clim.* 35, 2019–2034.
- Washington, R., James, R., Pearce, H., Pokam, W.M., Moufouma-Okia, W., 2013. Congo Basin rainfall climatology: can we believe the climate models? *Philos. Trans. R. Soc. B* 368, 20120296.
- Wheeler, M., Hendon, H.H., 2004. An all-season real-time multivariate MJO index: Development of an index for monitoring and prediction. *Mon. Wea. Rev.* 132, 1917–1932.
- Yang, G.-Y., Slingo, J., 2001. The diurnal cycle in the tropics. *Mon. Weather Rev.* 129, 784–801.
- Zaitchik, B.F., 2017. Madden-Julian Oscillation impacts on tropical African precipitation. *Atmos. Res.* 184, 88–102.
- Zhang, C., 2005. Madden-Julian Oscillation. *Rev. Geophys.* 43, RG2003.
- Zhang, C., Dong, M., 2004. Seasonality of the Madden-Julian oscillation. *J. Clim.* 17, 3169–3180.
- Zhou, L., et al., 2014. Widespread decline of Congo rainforest greenness in the past decade. *Nature* 509, 86–90.
- Zipser, E.J., Cecil, D.J., Liu, C., Nesbitt, S.W., Yorty, D.P., 2006. Where are the most intense thunderstorms on earth? *Bull. Am. Meteorol. Soc.* 87, 1057–1071.